Research Article

Nikolay Koshev*, Nikolay Yavich, Mikhail Malovichko, Ekaterina Skidchenko and Maxim Fedorov

FEM-based Scalp-to-Cortex EEG data mapping via the solution of the Cauchy problem

Abstract: We propose an approach and the numerical algorithm for mapping the electroencephalographic (EEG) data from the scalp to the cortex. The algorithm is based on the solution of ill-posed Cauchy problem for the Laplace's equation using tetrahedral finite elements. The FEM-based scheme allows to calculate the volumetric distribution of a potential over the head volume. We demonstrate the usage of the the algorithm for accurate estimation of the depth of electric sources in the head. The algorithm sufficiently increases the spatial resolution of the EEG technique making it comparable with intracranial techniques.

Keywords: Cauchy problem, data mapping, ill-posed problem, source localization, super resolution

MSC 2010: 35R25, 65N20, 35J99, 31B05, 31B20

1 Introduction

The majority of existing methods for electroencephalographic (EEG) data processing and source analysis falls into the following categories: parametric inversions (the dipole fitting), current-reconstruction methods (see, e.g., [2, 16, 18, 26, 31, 32]) and, somewhat less frequently, beamforming methods (see, e.g., [19, 28, 35, 37]). The approaches are very different (sometimes, fundamentally). All of them, however, use the EEG measurements as input data and, thus, highly depend on its quality.

The measured electric potential is strongly distorted by outer (with respect to the brain) head tissues. In biomedical applications, the conductivity distribution over the head tissues varies within a considerable interval. For example, the conductivity of the brain is about one order greater than the conductivity of the tissues located outside the brain (see, e.g., [23, 30]). This fact causes distortion of the electric potential measured on the outer surface of the domain (head). The current research is aimed to improve the quality of EEG data, partially excluding the influence of the outer tissues on the EEG signal.

Since the outer compartments (tissues) do not contain any sources producing the objective signal, the electric potential related to the brain sources satisfies the Laplace's equation there. Measuring the potential on the part of the head surface makes it possible to state the Cauchy problem for the Laplace's equation in order to map the data from the scalp to the brain surface. Such mapping is an auxiliary problem, allowing to sufficiently increase the accuracy of source localization due to better quality and spatial resolution of input data.

*Corresponding author: Nikolay Koshev CDISE, Skolkovo Institute of Science and Technology, Nobel st. 3, Moscow, Russia, e-mail: n.koshev@skoltech.ru
Nikolay YavichMikhail Malovichko CDISE, Skolkovo Institute of Science and Technology, Nobel st. 3, Moscow; and Applied Computational Geophysics Lab, Moscow Institute of Physics and Technology, 9 Institutskiy per. Dolgoprudny, 141701 Russia, e-mail: n.yavich@skoltech.ru, m.malovichko@skoltech.ru
Ekaterina SkidchenkoMaxim Fedorov CDISE, Skolkovo Institute of Science and Technology, Nobel st. 3, Moscow, Russia, e-mail: e.skidchenko@skoltech.ru, m.fedorov@skoltech.ru

The Cauchy problem for the data mapping in the context of EEG was considered in [9], where authors propose to use the boundary element method (BEM) in order to construct the cost functional for further minimization of it. The BEM, however, has some drawbacks related to the geometry of the calculation domain and method accuracy in comparison with finite element method (FEM) (see, e.g., [1, 13]).

In the current paper, we use the technique based on the mixed quasi-reversibility (MQR) method with linear finite elements proposed by L.Bourgeois in [5]. The method allows to reduce the Cauchy problem to a system of linear equations per compartment, built using two regularization parameters, the choice of which is also considered in [5, 6]. As we show later, the application of our algorithm enables us to "focus" a measured signal, sufficiently improving its spatial resolution even in complicated cases of in-brain source currents.

We also stress on the fact that the potential is being calculated not only on interfaces. Applying the proposed algorithm, we reconstruct the volumetric potential distribution over the head subdomains, which do not contain electric sources. Surprisingly, the considered technique can be used also for estimation of the depth of the electric sources, which fact makes possible to state a set of important problems like estimation of the cortex form (without MRI/CT images) or estimation of the electric conductivity of the head tissues. The latter one varies in a wide range depending on many factors: the employed method, the tissue temperature (room or body), the applied current frequency and the measurement condition (i.e., in vivo, in vitro or ex vivo), as well as the participant demographics (age, pathology) (see [27]).

Regarding practical use of the proposed method, it can be applied either directly to detect active parts of the cortex or as an intermediate procedure to propagate data from scalp to cortex before employing other processing techniques. Though, in this study, we focused only on mathematical and numerical aspects, we believe that the proposed method may serve as a basis for fast and accurate algorithms for analysis of real EEG data.

The paper is organized as follows. In Section 2, we describe the conductivity model of the human head, discuss the approximations being used and write out the governing equation of the EEG. In Section 3, we discuss the Laplace's equation for the sourceless compartments of the head and present some important notes about our implementation of the MQR method. Also, in the same section, we present our both proved and heuristic criteria for estimation of the source on the base of Cauchy problem solutions. Section 4 presents some numerical results and discussion. Concluding remarks are given in Section 5.

2 Mathematical description of EEG

This section is aimed to introduce the notations, which will be used in the paper, and remind the reader about some aspects of EEG together with its assumptions and equations.

2.1 The computational domain and sources

The head volume in general and the brain in particular consist of many parts and organs: scalp, skull bone, cerebrospinal fluid (CSF), the brain itself and its components. Using the macroscopic approximation, we assume the conductivity to be identical across the particular compartment of the head, i.e., we expect the conductivity to be the piecewise-constant distribution over the computational domain.

Consider the domain $\Omega \subset \mathbb{R}^3$ with a piecewise-smooth boundary $\partial\Omega$. The domain under consideration represents the volume of the head and is assumed to consist of several subdomains

$$\Omega_i, \ i = 1, \ldots, N_d: \quad \Omega = \bigcup_{i=1}^{N_d} \Omega_i,$$

representing N_d organs inside the head (see Figure 1 (a). Each organ is expected to have a constant electric conductivity $\sigma_i, i = 1, \ldots, N_d$ (see [23]). We further assume a nested domain topology of the introduced partitioning.
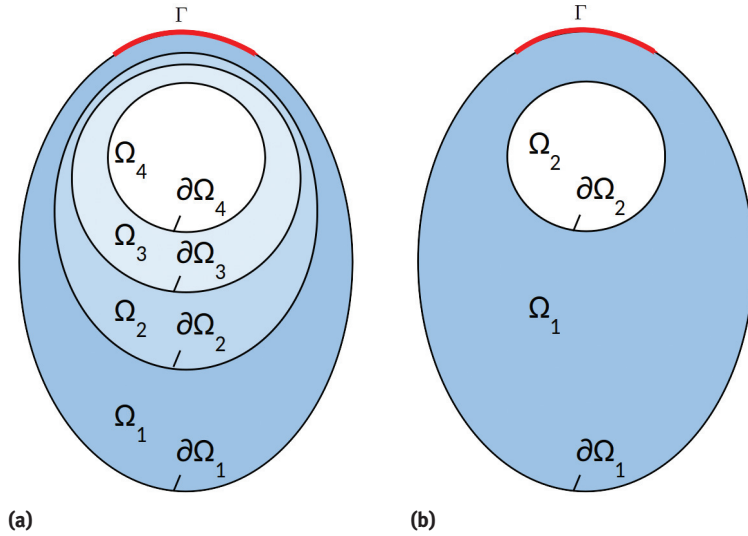
Figure 1: Computational domains and boundaries: (a) the nested domains topology; (b) the simplified model used in the current work. The measurement area Γ is highlighted with the thick red line.

The conductivities of outer (with respect to the human brain) tissues are much lesser than the conductivity of the brain itself (see, e.g., [23, 30]). We also note that the area of measurements in the case of EEG is located at the top of a head, which leads to respectively small thickness of those outer tissues. Regarding to this facts, for simplicity, we take into account only simple head model consisting of two domains (see Figure 1 (b)): the brain is represented by the inner domain Ω_2 with the conductivity σ_2 equal to the conductivity of the cortex, and the outer tissues (scalp, skull, cerebrospinal fluid, etc.) are described by the only one outer domain Ω_1 with averaged conductivity σ_1. We noticed in our numerical experiments that this simplification leads to respective error 2 % to 4 % in our calculations. Thus, this simplification can be applied to real (experimental) data. Further, in order to make the presentation clearer, we will consider only the latter structure.

We denote the outer boundary of each domain Ω_m as $\partial\Omega_m$ for $m = 1, 2$. For convenience, indexing can be done starting from outer domain representing scalp, skull and CSF to inner one representing the brain. In such a way, the outer domain Ω_1 is bounded by the surfaces $\partial\Omega_1$ (outer surface) and $\partial\Omega_2$ (inner surface). The outer head surface in such indexing is $\partial\Omega \equiv \partial\Omega_1$.

In the EEG technique, the measurements are being performed in a bounded area of the surface located commonly at the top of a head. In further consideration, this part of the boundary, which we call *accessible part of the boundary*, is represented by the portion of the outer surface $\Gamma \subset \partial\Omega_1$ (see Figure 1).

For further discussion we also need to introduce the rest of the boundary Π of the subdomain Ω_1, which we call *inaccessible part of the boundary*. This portion contains unknown data, which we will need to restore

$$\Pi = (\partial\Omega_1 \setminus \Gamma) \cup \partial\Omega_2.$$

EEG method measures the electric potential generated by the biochemical currents inside the head. There are two main kinds of such currents: currents generated by the brain and the muscle currents. Since the EEG technique aims to study the electric activity of the brain, the signal of interest is generated by brain currents. Muscle currents have much higher frequencies and thus can be easily filtered. Therefore, we can assume the current sources are located only inside the brain (more accurately - on the brain surface), while all other areas do not contain electric sources: supp $\mathbf{J}(\mathbf{x}) \subset \Omega_2$.

Remark 2.1. Real EEG measurements are being provided with a device consisting of some number of electrodes (channels). After measurement, the data processing may include or not include the interpolation (so-called channel interpolation) in order to obtain the signal not only in particular points – sensors positions, but also at each point of measurement area Γ. There is a number of works devoted to such interpolation

(see, for example, [10, 11, 29, 36]), which take into account the shape of the head, properties of harmonic functions, etc. In the current article we, however, do not consider these procedures, assuming the signal be already interpolated and, consequently, known at each point $\mathbf{x} \in \Gamma$.

2.2 Governing equation

As mentioned above, the conductivity $\sigma(\mathbf{x})$, $\mathbf{x} \in \Omega$, is assumed to be a piecewise-constant function over the volume under consideration (head). The conductivity of the media outside the head expected to be zero:

$$\sigma(\mathbf{x}) = \begin{cases} \sigma_i, & \mathbf{x} \in \Omega_i \subset \Omega, \\ 0, & \mathbf{x} \notin \Omega. \end{cases}$$

Given the frequencies of the neural currents within the interval of 1–100 Hz, the quasi-static approximation is justified. This was proved in numerous well-known works on EEG, e.g., [13, 17, 33, 34, 38].

Let the volumetric distribution of a primary neuronal current density (the source) be denoted as $\mathbf{J}^p$. Under the assumptions, the electric potential $U(\mathbf{x})$ satisfies the equation

$$\nabla \cdot (\sigma \nabla U) = \nabla \cdot \mathbf{J}^p, \quad \mathbf{x} \in \Omega. \tag{2.1}$$

The potential further satisfies the zero Neumann boundary condition on $\partial\Omega$:

$$\mathbf{n} \cdot \nabla U = 0, \quad \mathbf{x} \in \partial\Omega. \tag{2.2}$$

The zero Neumann boundary condition follows from the assumption of zero conductivity of the media outside the head [13].

We assume the existence of the *accessible part of the boundary* $\Gamma \subset \Omega$ (described in Section 2.1), on which the electric potential $U(\mathbf{x})$ is known:

$$U|_\Gamma = u(\mathbf{x}), \quad \Gamma \subset \partial\Omega \subset \mathbb{R}^3. \tag{2.3}$$

Remark 2.2. Equation (2.1) contains the conductivity coefficient $\sigma(\mathbf{x})$, which can be obtained using adjustment of known conductivity values with the images of geometry of the tissues, obtained with the magnetic resonance imaging (MRI) or computed tomography (CT). There are also other techniques for conductivity distribution acquisition. Additionally, some standard models of such distribution are often employed. Regardless of the approach, in the current work we assume the distribution $\sigma(\mathbf{x})$ to be known at every point $\mathbf{x} \in \Omega$.

3 The Cauchy problem for sourceless domain

Areas outside the brain volume consist of skin, skull bones, cerebrospinal fluid (CSF). We assume the objective signal be produced only by inner or surface brain currents. Thus, in our consideration we can expect that the tissues outside the brain do not contain any sources, an assumption which is important for further reasoning.

In sourceless homogeneous volume, equation (2.1) takes the form

$$\Delta U = 0, \quad \mathbf{x} \in \Omega_1 \tag{3.1}$$

Indeed, the equation above can be obtained from (2.1) by nulling the right-hand side due to absence of sources with the assumption that the conductivity $\sigma_1 = \text{const}$.

3.1 Statement of the problem

Equation (3.1) together with boundary conditions (2.2) and (2.3) enables us to state an auxiliary problem, which we name the *extrapolation problem*.

Extrapolation problem for the electric potential. *Assume the function $u(\mathbf{x})$, $\mathbf{x} \in \Gamma$, to be known. Find the function $U(\mathbf{x})$ such that*

$$\Delta U = 0, \qquad \mathbf{x} \in \Omega_1, \tag{3.2}$$

$$U|_\Gamma = u(\mathbf{x}), \quad \mathbf{x} \in \Gamma, \tag{3.3}$$

$$\mathbf{n} \cdot \nabla U|_\Gamma = g(\mathbf{x}), \quad \mathbf{x} \in \Gamma. \tag{3.4}$$

Remark 3.1. In biophysical applications, the interface between the brain and cerebrospinal fluid contains sources. Moreover, the mentioned interface is the only area, where the electric currents producing the objective signal are possible. Due to this fact, from the mathematics' point of view, the Cauchy problem for the Laplace's equation can be stated in this case only for open domain, which does not contain the brain surface itself. Despite this, our numerical experiments showed that its solution (i.e., backpropagation of the potential to the brain surface) is accurate enough and can be used in practice. This is caused by the fact we do not compute the potential only on boundary, but compute it in the whole sourceless domain. Thus, we can estimate the electric potential at the points arbitrary closed to the desirable surface. The respective numerical experiments will be shown in Section 4.

Remark 3.2. If we consider multiple nested sourceless domains instead of only one, we can also write the Dirichlet and Neumann boundary conditions for all of them:

$$U_i(\mathbf{x})|_{\partial\Omega_i} = u_i(\mathbf{x}),$$

$$\mathbf{n}\nabla U_i(\mathbf{x})|_{\partial\Omega_i} = \frac{\sigma_{i-1}}{\sigma_i}\mathbf{n}\nabla\widetilde{U}_i|_{\partial\Omega_i} \equiv g_i(\mathbf{x}),$$

where $\widetilde{U}_i$ denotes the potential on the outer side of the interface $\partial\Omega_i$, $i > 1$. The boundary conditions are obtained from requirements for potential and its normal derivative to be continuous inside the computational domain Ω. Assuming the conductivity $\sigma(\mathbf{x}) = 0$, $\mathbf{x} \notin \Omega$, we can easily obtain the zero Neumann condition (2.2), common for EEG problem.

The Cauchy problem for the Laplace's equation is one of the classical examples of an ill-posed problem. During the last years, a number of validated approaches to its solution were presented. The approaches can be divided into three main categories: approaches based on the optimization (Tikhonov's regularization, etc.), methods based on quasi-reversibility and iterative approaches (see, for example, [14]).

The first category includes classical Tikhonov's regularization [4, 25], which is well-established and mostly used. Conventional Tikhonov's regularization, however, has some issues with the solution accuracy (see, for example, [20]). Also, this category includes approaches based on the construction of a strictly convex Tikhonov-like functional weighted with a domain-depending Carleman weight function [3, 20]. Despite the great accuracy of the solution, the method, however, is rather hard to implement and is better suitable for nonlinear problems, for which it was designed. Other solutions based on optimization approaches are presented, for example, in [9]. The second category is probably the most known category of the approaches. It is based on the quasi-reversibility method, which is being used in order to state a weak formulation of a problem, which, after discretization, is turned into solving a linear system of algebraic equations. Some methods are presented, for example, in [5–8, 12].

3.2 The method

Equations (3.2)–(3.4) define the typical Cauchy problem for the Laplace's equation. Uniqueness of this problem was proved, for example, in[24]. Solution of the problem was considered in a set of works (see, for example, [3–5, 7, 8, 14, 25]).

In the current paper, we use the MQR method provided for linear finite-element approximations in [5, 6]. As one can see below, the method depends on two regularization parameters. The most efficient way of choosing the regularization parameters is the balancing principle, which is described in [7].

We introduce the following notations:

$$V_0 = \{h \in H^1(\Omega_1) : h|_\Gamma = 0\},$$
$$V_1 = \{h \in H^1(\Omega_1) : h|_\Pi = 0\}, \tag{3.5}$$
$$\tilde{V}_0 = \{h \in H^2(\Omega_1) : h|_\Gamma = u(\mathbf{x})\}.$$

Let $0 < \varepsilon \ll 1$ and $0 < \delta \ll 1$ be two fixed small numbers (regularization parameters).

Weak formulation of MQR method. *Find a pair of functions $(U, \lambda) \in \tilde{V}_0 \times V_1$ such that*

$$\varepsilon \int_{\Omega_1} \nabla U \cdot \nabla h \, dx + \int_{\Omega_1} \nabla h \cdot \nabla \lambda \, dx = 0 \quad \text{for all } h \in V_0, \tag{3.6}$$

$$\int_{\Omega_1} \nabla U \cdot \nabla \mu \, dx - \delta \int_{\Omega_1} \nabla \lambda \cdot \nabla \mu \, dx = 0 \quad \text{for all } \mu \in V_1. \tag{3.7}$$

In [5] one can find proofs of existence and uniqueness of the solution, its stability and convergence of the solution of (3.6)–(3.7) to the exact solution of problem (3.2)–(3.4) with $(\varepsilon, \delta) \to 0$ when the error in the input data $u(\mathbf{x}) \to 0$.

The finite element approximation. Among many different methods available (finite-difference, finite-volume, see, e.g., [22], finite element, etc.), we used the finite element method (FEM) with linear basis functions on tetrahedrons as it combines simplicity and flexibility.

Let X_h be the space of P_1 piecewise linear continuous finite-element basis functions with the basis $h_i(\mathbf{x})$, $i = 1, \ldots, N$ (here N is the number of nodes). Denote by N_Γ the number of nodes belonging to Γ. For convenience, we also introduce the notation $i(D) = \{i : \mathbf{x}_i \in D\}$ to be indices of nodes of a finite element mesh, which belong to some domain $D \subset \mathbb{R}^3$.

Introduce the following subspaces, which are the finite-dimensional analogs of the corresponding subspaces (3.5):

$$X_0 = \{h \in X_h : h|_\Gamma = 0\},$$
$$X_1 = \{h \in X_h : h|_\Pi = 0\},$$
$$\tilde{X}_0 = \{h \in X_h : h - U_0 \in X_0\}.$$

Here U_0 is the approximation of the function with the following properties:

$$U_0|_\Gamma = u(\mathbf{x}),$$
$$\partial_n U_0|_\Gamma = 0,$$
$$U_0 \in H^1(\Delta, \Omega),$$

where

$$H^1(\Delta, \Omega) = \{U \in H^1(\Omega) : \Delta U \in L^2(\Omega)\}.$$

The formulation of the MQR method is still the same as (3.6)–(3.7) with the difference that the pair of functions to be found now belongs to $(U, \lambda) \in \tilde{X}_0 \times X_1$. Finite-dimensional approximations of U and λ can be written as follows:

$$U(\mathbf{x}) \approx \sum_{i=0}^{N} U_i h_i(\mathbf{x}), \quad \mathbf{x} \in \Omega_1, \tag{3.8}$$

$$\lambda(\mathbf{x}) \approx \sum_{i=0}^{N} \lambda_i h_i(\mathbf{x}), \quad \mathbf{x} \in \Omega_1. \tag{3.9}$$

For convenience, introduce the following notation:

$$A_{im} = \int_{\Omega} \nabla h_i(\mathbf{x}) \cdot \nabla h_m(\mathbf{x}) dx, \quad i, m = 1, \ldots, N.$$

Substituting (3.8)–(3.9) into (3.6)–(3.7) with $h = h_j \in X_0, \mu = h_k \in X_1$, we obtain

$$\varepsilon \sum_{i(\Omega_1)} U_i A_{im} + \sum_{j(\Omega_1)} \lambda_j A_{jm} = 0, \quad m = m(\Omega_1 \setminus \Gamma), \tag{3.10}$$

$$\sum_{l(\Omega_1)} U_l A_{lk} - \delta \sum_{n(\Omega_1)} \lambda_n A_{nk} = 0, \quad k = k(\Omega_1 \setminus \Pi). \tag{3.11}$$

Since $U(\mathbf{x}) \in \tilde{X}_0$, we can state that $U_i = u_i, i \in i(\Gamma)$, and the first term of (3.10) takes the form

$$\varepsilon \sum_{i(\Omega_1)} U_i A_{im} = \varepsilon \sum_{i(\Omega_1 \setminus \Gamma)} U_i A_{im} + \varepsilon \sum_{i(\Gamma)} u_i A_{im}, \quad m \in m(\Omega_1 \setminus \Gamma).$$

Since the function $\lambda(\mathbf{x}) \in X_1$, the second term can be written as follows:

$$\sum_{j(\Omega_1)} \lambda_j A_{jm} = \sum_{j(\Omega_1 \setminus \Pi)} \lambda_j A_{jm}.$$

Reasoning in the same way, we obtain for both equations (3.10) and (3.11) that one can rewrite these equations as follows:

$$\varepsilon \sum_{i(\Omega_1 \setminus \Gamma)} U_i A_{im} + \sum_{j(\Omega_1 \setminus \Pi)} \lambda_j A_{jm} = a_m, \quad m = m(\Omega_1 \setminus \Gamma), \tag{3.12}$$

$$\sum_{l(\Omega_1 \setminus \Gamma)} U_l A_{lk} - \delta \sum_{n(\Omega_1 \setminus \Pi)} \lambda_n A_{nk} = b_k, \quad k = k(\Omega_1 \setminus \Pi), \tag{3.13}$$

where

$$a_m = -\varepsilon \sum_{i(\Gamma)} u_i A_{im}, \quad m \in m(\Omega_1 \setminus \Gamma), \tag{3.14}$$

$$b_k = - \sum_{i(\Gamma)} u_i A_{ik}, \quad k \in k(\Omega_1 \setminus \Pi). \tag{3.15}$$

Denote the number of nodes located in some domain D as N_D. It is easy to see that in the representation above the discrete system contains $2N_\Omega - N_{\partial\Omega}$ equations and the same number of variables. It is thus can be solved by an iterative solver. Thus, the final system can be written in the form

$$\begin{pmatrix} A^{11} & A^{12} \\ A^{21} & A^{22} \end{pmatrix} \begin{pmatrix} U \\ \lambda \end{pmatrix} = \begin{pmatrix} a \\ b \end{pmatrix},$$

where notations $A^{rt}, r, t = 1, 2$, represent parts of the matrix A, defined with the changing of i, j, m, l, k, n in (3.10)–(3.11), and a, b are vectors defined by (3.14)–(3.15).

3.3 Estimation of the depth of the source under the surface

In this subsection, we present the main idea of the source localization using the Cauchy solution for the Laplace equation. We consider a source inside a homogeneous volume bounded by the scalp and cortical surfaces. Despite the fact that this approximation does provide accurate values of potential, we show that under an appropriate set of assumptions, common for electroencephalography, our results apply to EEG.

Homogeneous volume. In the current paragraph we assume the head volume to be homogeneous. As before, we denote by Ω the domain representing the head volume, and represent it with a set of N_d nested subvolumes Ω_k such that $\bigcup_{k=1}^{N_d} \Omega_k = \Omega$, and $\Omega_k \cap \Omega_{k+1} = \partial\Omega_{k+1}$ for all $k = 1, \ldots, N_d - 1$. Assume the head volume outside the brain to be homogeneous. Thus, the choice of subdomains Ω_k does not depend on the "real" layers (representing different tissues) of the head, which fact allows us to build these domains such that the its boundaries be as close to each other as it is possible in order to get the accuracy gain. The measurable part of the boundary is $\Gamma \subset \partial\Omega$.

Consider now a set of volumes $\Theta_i = \bigcup_{k=1}^{i} \Omega_k$. Thus, $\Theta_{i-1} \subset \Theta_i$ for all $i \leq N_d$. For simplicity, we also introduce the notation $f = \nabla \cdot \mathbf{J}$, $f \in L^2(\Omega)$ for the right-hand side of equation (2.1) and assume that there exists an $s > 1$ such that supp$(f) \cap \Theta_i = \varnothing$ for all $i < s$ (i.e., we assume the first $s - 1$ domains Θ_i to be sourceless). The potential U in the domain Ω satisfies equation (2.1) with the boundary condition (2.2), but for generality we denote by U some function, which satisfies only equation (2.1). Let $u(\mathbf{x}) = U|_\Gamma$, and $q(\mathbf{x}) = (\partial_n U)|_\Gamma$.

Now consider a set of functions U_i, $i = 1, \ldots, N_d$, satisfying the following set of Cauchy problems:

$$\Delta U_i(\mathbf{x}) = 0, \quad \mathbf{x} \in \Theta_i, \tag{3.16}$$

$$U_i(\mathbf{x})|_\Gamma = u(\mathbf{x}), \quad (\partial_n U_i(\mathbf{x}))|_\Gamma = q(\mathbf{x}). \tag{3.17}$$

We assume that the solutions of problems (3.16)–(3.17) exist for all $i \leq N_d$. Note that uniqueness of the solution of the last problem is proven (see [5]). We formulate the following proposition.

Proposition 3.1. *With the above assumptions, the functions $U_i(\mathbf{x})$ and $U(\mathbf{x})$ coincide in the domain Θ_i, i.e.,*

$$\|U - U_i\|_{L^2(\Theta_i)} = 0 \quad \text{for all } i < s.$$

Proof. Consider the function $v = U - U_i$. This function satisfies the problem

$$\Delta v_i(\mathbf{x}) = f(\mathbf{x}), \ x \in \Theta_i, \quad v_i(\mathbf{x})|_\Gamma = 0, \quad (\partial_n v_i(\mathbf{x}))|_\Gamma = 0.$$

Referring to the assumption supp$(f) \cap \Theta_i = \varnothing$ for all $i < s$, we rewrite the last problem

$$\Delta v_i(\mathbf{x}) = 0, \ x \in \Theta_i, \quad v_i(\mathbf{x})|_\Gamma = 0, \quad (\partial_n v_i(\mathbf{x}))|_\Gamma = 0.$$

Due to [5, Lemma 1], the solution $v_i \equiv 0$, $i < s$, is unique, which proves the current proposition. $\qquad\square$

It is important to note that due to Proposition 3.1 we can consequently conclude that $\|U_{i-1} - U_i\|_{L^2(\Theta_{i-1})} = 0$ for all $i < s$. Thus, while there is no source in the computational domain, the solution of the Cauchy problem on the certain iteration coincides with the one on the previous iteration.

It is reasonable to expect that $\|U_{s-1} - U_s\|_{L^2(\Theta_{s-1})} > 0$, i.e., the solution starts differ from the solution on the previous iteration, when the computational domain starts to contain the source. Unfortunately, it is impossible to prove this in general case, without imposition of the additional assumptions on the function f. Our numerical experiments presented in Section 4 always show, however, expectable jump of the norm $\|U_{s-1} - U_s\|_{L^2(\Theta_{s-1})} > 0$, which allows us to formulate the following algorithm.

Algorithm 1. Algorithm for estimation of the depth of the source under the surface.

Define a tetrahedral mesh and subdomains Θ_i, $i = 1, \ldots, N_d$.

Solve the Cauchy problem (3.16)–(3.17) for $i = 1$ in order to obtain the function U_1.

for $i = 2, \ldots, N_d$ **do**

    Calculate U_i solving the Cauchy problem (3.16)–(3.16).

    Calculate the number $e_i = \|U_{i-1} - U_i\|_{L^2(\Theta_{i-1})}$.

end

Find the index i in which $e_i - e_{i-1} > l$, where $l > 0$ is some number, chosen, for example, as a mean value over e_i.

The index $i \equiv s$ due to the consideration above.

Indeed, solving the Cauchy problem for each of subdomains Θ_i, and calculating the norms

$$e_i = \|U_{i-1} - U_i\|_{L^2(\Theta_{i-1})},$$

we expect to observe the jump of e_i value at the number $i = s$. The described algorithm will be shown below, in Section 4.

Remark 3.3. One can see that all the facts we discuss in the above paragraph can be proven only when the corresponding equations have a solution; we, however, note that existence of the solution of the Cauchy problems (3.16)–(3.17) guaranteed physically for $i < s$ due to the Proposition 3.1. Indeed, the solution U_i coincides in the calculation domain Θ_i with the solution of the Poisson's equation (2.1) with zero

Neumann boundary condition, which is always solvable in the assumption $f \in L^2(\Omega)$. We cannot guarantee the existence of the solutions $U_s(\mathbf{x})$. Predictable, our numerical experiments show in the last case the same jump of the consequence e_i. In order to be more accurate, we can also use the considered criterion together with the one based on the dependence of the generalized residual of system (3.10)–(3.11), which criterion will be shown in further consideration.

Other criteria. In order to justify the idea, we propose to use the algorithm together with some other heuristic criteria. It is impossible to prove the criteria below strictly mathematically, but these criteria are still being rather *physical*, and, we believe, enough trusted.

First of all, we consider also the overall residual r_i of system (3.12)–(3.13) after the solution of the Cauchy problem (3.16)–(3.17). It is proven in [5] that the MQR method converges to the unique solution U_i if it exists. Thus, the generalized residual should be comparatively close to zero. Since the solutions U_i exist for any $i < s$, we expect to see the jump of r_i for $i = s$.

We also refer to the fact that MQR method, described above in the article, aims to find two distributions: $U(\mathbf{x})$, corresponding to the potential, and $\lambda(\mathbf{x})$, which represents the Laplacian $\Delta U(\mathbf{x})$. For electric potential mapping, we used only the first parameter, but now we propose to consider also the second one. Consider the sequence $\lambda_i(\mathbf{x}) \equiv \Delta U_i(\mathbf{x})$. Thus, we also can expect the jump in the norm $d_i = \|\lambda_i\|_{L^2(\Omega_i)}$ for $i = s$.

Also, one more criteria can be considered. Obviously, the absolute value of the electric potential reaches its maximum on the boundary of the domain Θ_i, which is located on the closest distance from the source. Denote the described value by $m_i = max(U_i|_{\Theta_i})$. Our numerical experiments show us the maximum value of the latter consequence always located in the domain Θ_{s-1}.

All considered criteria will be shown below, in Section 4.

Heterogeneous media. In most real-life applications (including the case of encephalography, which is under the consideration in the current paper), we need to find the source not in an idealized homogeneous volume. Talking about the encephalography, the sourceless subdomains of the head consist of different kinds of tissues, being characterized with different conductivities; moreover, the conductivity may vary in dependence on a big number of factors. However, our numerical experiments show that the considered criteria may be applied for an inhomogeneous volume. This becomes possible because we consider in this case only behavior of the difference between potentials, reconstructed in different calculation areas instead of the precise potential distribution in these areas. Regarding the above consideration, we were using only a homogeneous media, without any information of real distribution of conductivity. Thus, applying the formulated "homogeneous" algorithm to inhomogeneous volume Ω, we still will have the same behavior of the e_i sequence, but the Cauchy conditions should be different for homogeneous and heterogeneous cases. Our numerical experiments show, however, high accuracy of the estimation of the depth even in heterogeneous volume. We explain the observed results with the fact that in case of encephalography all sourceless volumes are dielectrics with very low conductivities; despite the fact conductivities of different tissues are not equal to each other, they are rather close. Moreover, thickness of the sourceless layers is relatively small under the area of measurements, located at the top of a head. Thus, we do not expect big change in the Cauchy conditions due to heterogeneity of the object. Our numerical experiments show that the relative difference in Cauchy data between these two cases is about 1 % to 4 %. The numerical experience on stability of the algorithm, shown in Section 4, allows to expect the comparable additional error in the reconstructed potential, and in estimated depth of the source consequently.

4 Numerical results

The current section is aimed to present the numerical results of the algorithm described above. We start with two cases of the simple model representing the brain with the inner sphere, and outer tissues with the outer spherical layer. Then we present the numerical results for a more realistic model of the head, based on simplified MRI data [15]. In the current paper, we use simulated data. The simulations were implemented with

the finite element numerical solution of equation (2.1) for the sources/conductivity distributions presented below. The SLAE (3.10)–(3.11) has been solved using the generalized minimal residual (GMRES) method converging to the residual 10^{-6}. All calculations in the current section have been provided using a laptop equipped with 16 Gb RAM and CPU Intel Core-i7 7820HQ.

4.1 Spherical model with the sources located under the surface of the active domain

The case considered in this subsection is unrealistic since the currents here are located under the surface of the "active" domain. In truth, the biochemical sources are placed on the interface between a brain and cerebrospinal fluid, i.e., on the brain surface. In this case, in the strict sense, the Cauchy problem for the Laplace's equation cannot be stated. Thus, we find it reasonable to start the presentation of our numerical results in the strict case when the sourceless domain is closed, i.e., its boundaries are also sourceless.

The head here is represented with a simple model, which consists of the spherical "active" domain Ω_2 with the radius $r_2 = 0.8$ and a spherical layer representing the outer sourceless area Ω_1 with the radius $r_1 = 1$. The conductivity of the inner domain is $\sigma(\Omega_2) = \sigma_2 = 2.2$ S/m, and the domain Ω_1 can be characterized with the conductivity $\sigma(\Omega_1) = \sigma_1 = 0.1$ S/m. The electric sources are depicted with the support (three spots) on Figure 2 (a). The support spots contain the constant currents inside it: $\mathbf{J}(\mathbf{x}) = (0, 10^{-7}A, 0)$, $\mathbf{x} \in \text{supp}(\mathbf{J})$.

The finite element mesh for the sourceless domain Ω_1 consists of $484,946$ tetrahedra and $90,435$ vertices. The calculation time for the Cauchy problem solver implemented with the Matlab is equal to 5.7 seconds.

Figure 2 (a) and (b) depict the simulated electric potential on the outer surface and the surface of the "active" domain, respectively, while (c) and (d) show respectively the simulated potential on the "brain" surface, and the result of its reconstruction using the algorithm presented above.
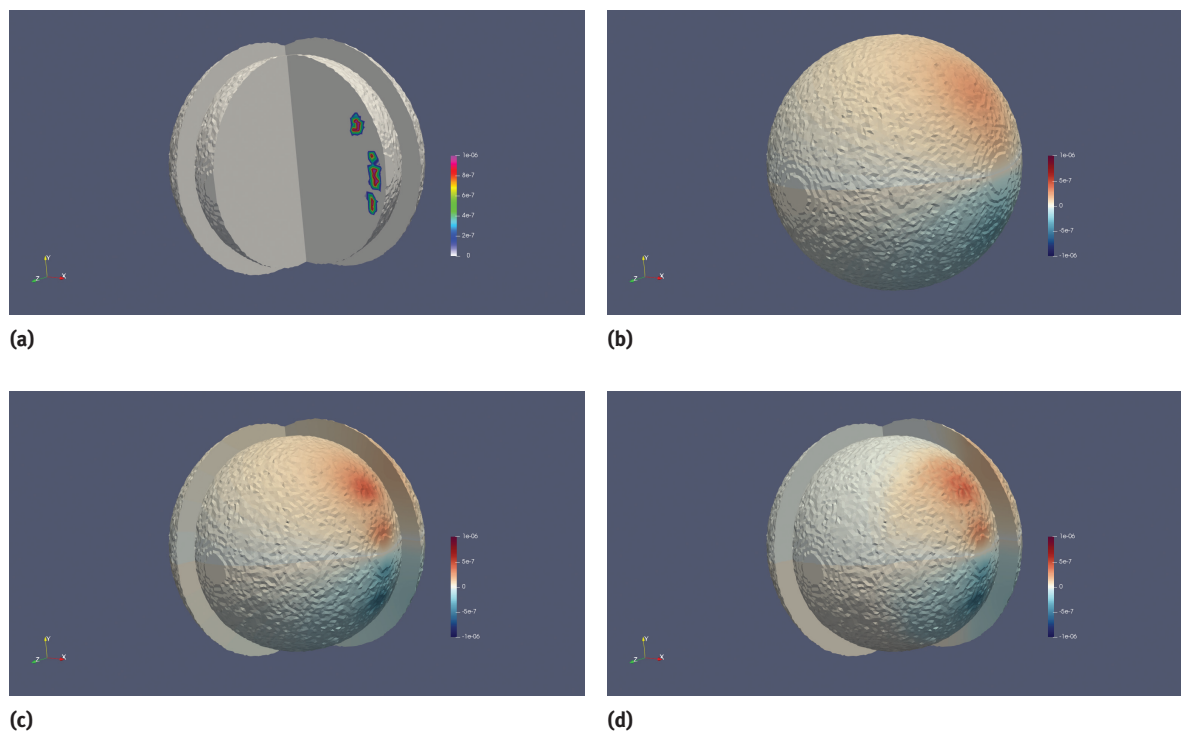

(a)

(b)

(c)

(d)

Figure 2: Spherical model (sources located under the surface of the active domain): (a) simulation of the electric potential on the outer surface (scalp); (b) simulation of the electric potential on the "active" domain surface; (c) simulation of the potential on the surface of the inner sphere; (d) the potential on the inner sphere surface mapped from the data depicted in (b) via the solution of the Cauchy problem ($\varepsilon = 0.0001$ and $\delta = 0.001$).
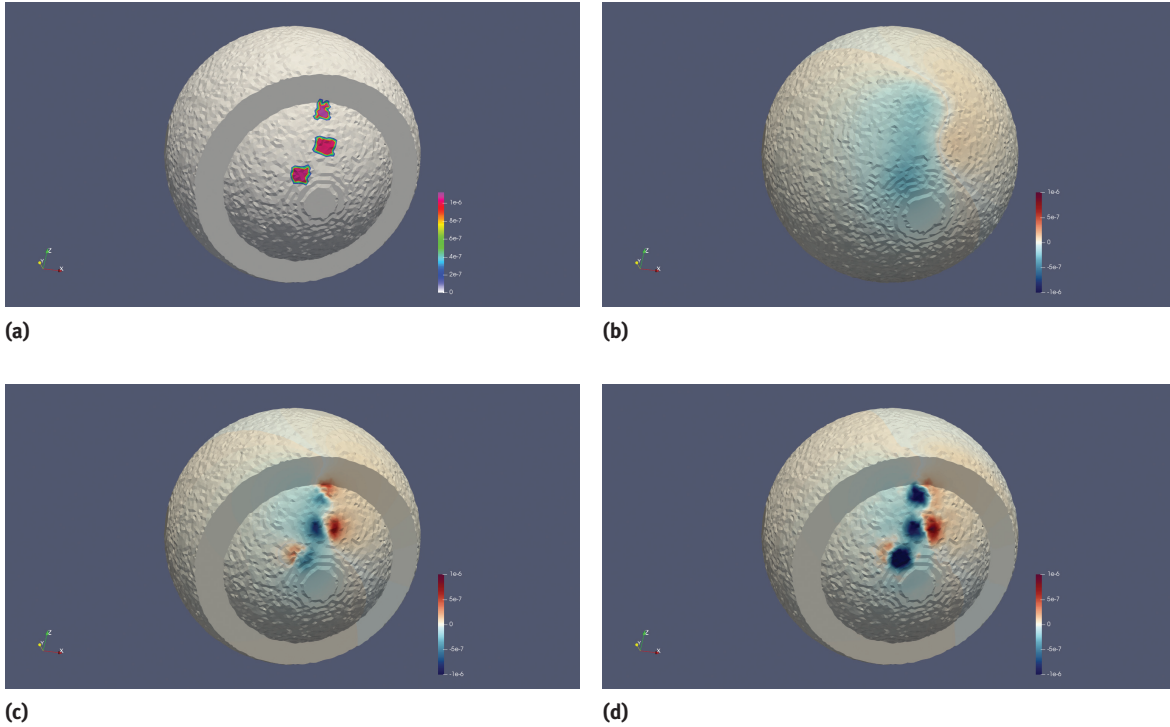
(a)

(b)

(c)

(d)

Figure 3: Spherical model (sources located on the surface of the inner sphere): (a) The current density (sources); (b) simulation of the electric potential on the outer surface (scalp); (c) simulation of the electric potential on the "active" domain surface; (d) the potential on the inner sphere surface, obtain via solution of the Cauchy problem with regularization parameters $\varepsilon = 0.00001$ and $\delta = 0.001$.

4.2 Spherical model: More realistic case

Geometrically, the model under consideration in the current subsection is identical to the one in the previous subsection. It is also characterized by the same conductivity distribution. The difference is in the current. First of all, the currents here are located on the interface between active and inactive domains, which is closer to the real-life encephalographic situation. Strictly speaking, the domain Ω_1, in this case, should not contain its $\partial\Omega_2$ boundary surface, and it should be the opened domain. However, since the potential can be calculated via the solution of the Cauchy problem for the surface, which is arbitrary close to the surface $\partial\Omega_2$, we were not surprised that the modelled and restored via the Cauchy problem solution potentials on an active domain surface are relatively close to each other. The following results can be seen in Figure 3.

The finite element mesh for the sourceless domain Ω_1 consists of 484,946 tetrahedra and 90,435 vertices. The calculation time for the Cauchy problem solver implemented with the Matlab is equal to 5.7 seconds.

4.3 Simplified head model based on real MRI data

The model described in this subsection is a simplified but more realistic model of the head. The mesh was constructed using the iso2mesh software [15]. Here the "realistic" distribution of the current density over the brain surface was used.

In order to make the result more realistic, we employed two kinds of current density distributions. Figure 4 depicts the model with several "active" spots (support areas) of the cortex, where the current, corresponding to the spot is constant inside it. Figure 5 shows the situation when the current is randomly defined at each point inside the support areas (areas itself are similar to the previous case).
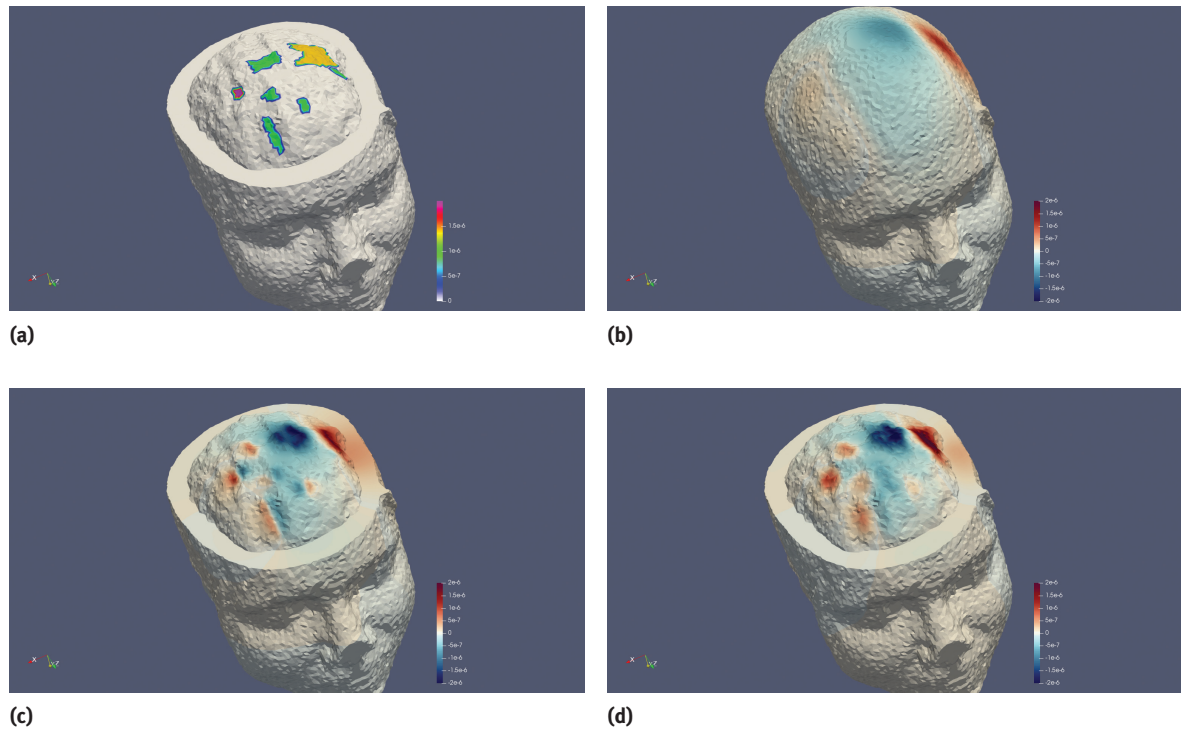
(a)

(b)

(c)

(d)

Figure 4: MRI-based model of the head: case with piecewise-constant current distribution on the brain surface. (a) the current, (b) FEM-simulated potential on the outer surface of the head (input data for the Cauchy problem, (c) FEM-simulated potential; (d) reconstruction of the potential on the brain surface on the base of the data depicted by (b).
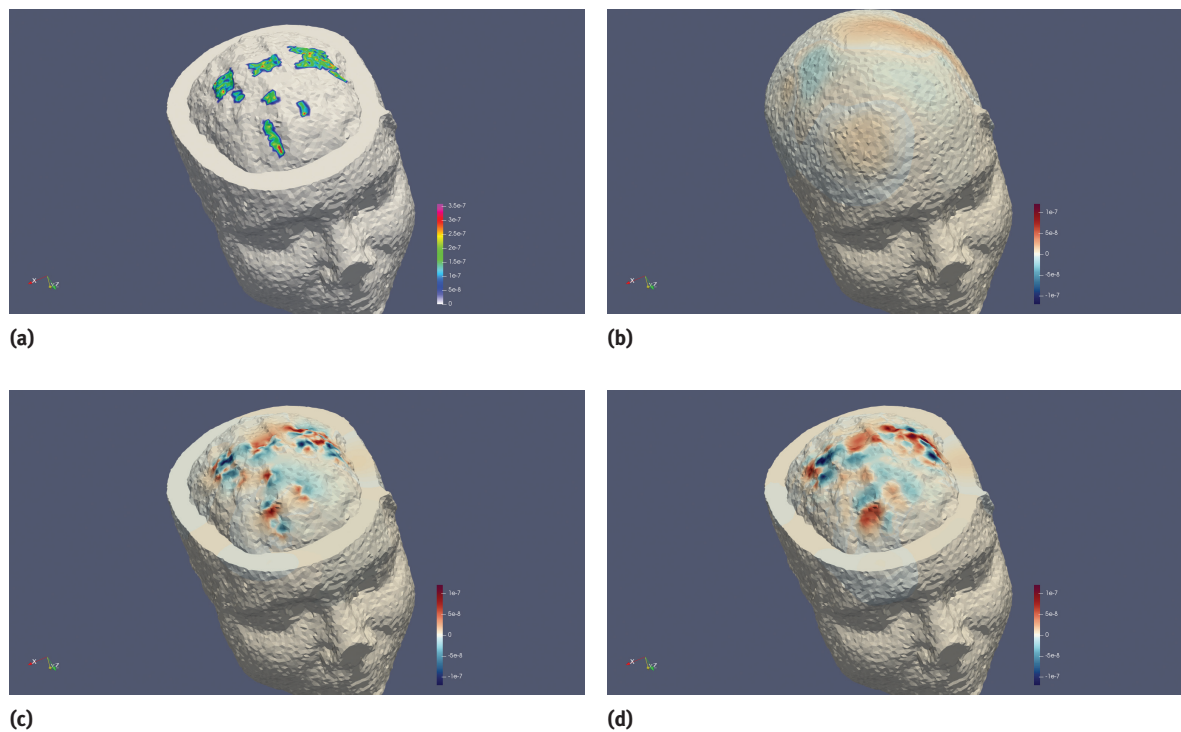

(a)

(b)

(c)

(d)

Figure 5: MRI-based model of the head: case with random current, distributed within big areas of the brain surface. (a) the current, (b) FEM-simulated potential on the outer surface of the head (input data for the Cauchy problem, (c) FEM-simulated potential; (d) reconstruction of the potential on the brain surface on the base of the data depicted by (b).

The finite element mesh for the sourceless domain Ω_1 consists of 444,916 tetrahedra and 82,239 vertices. The calculation time for the Cauchy problem solver implemented with Matlab varies in the interval 6−11 seconds in dependence of the current distribution used for modelling.

4.4 Discussion of the numerical results

Current paragraph is devoted to discussion of obtained numerical results including error analysis, stability and choice of the tetrahedral mesh density. Also, we will stress here one interesting factor we observed, which makes possible the idea of electric source localization on the base of measured potential only. All the benchmarks in the current paragraph were applied to spherical models due to simplicity of building of suitable meshes, simplicity of implementation of the benchmarks, and comparatively small calculation times.

In our benchmark for error analysis, we used the spherical model, described in Section 4.1. Adding Gaussian noise with varying amplitude, we calculated the error E_{Cauchy} (4.1) in the Cauchy solution and the error E_{input} in the input data (4.2):

$$E_{\text{Cauchy}} = \frac{\|U|_{\partial\Omega_{N_d}} - U^*|_{\partial\Omega_{N_d}}\|_{L_2}}{\|U^*|_{\partial\Omega_{N_d}}\|_{L_2}}, \tag{4.1}$$

$$E_{\text{input}} = \frac{\|U_\Delta|_\Gamma - U^*|_\Gamma\|_{L_2}}{\|U^*|_\Gamma\|_{L_2}}, \tag{4.2}$$

where $U_\Delta|_\Gamma$ represents the noisy measured potential, U^* represents the ground-true solution (i.e., result of direct modelling of a potential in the entire volume Ω), and $U|_{\partial\Omega_{N_d}}$ represents the potential, restored with the Cauchy problem solution. Here $N_d=2$. The dependence of these errors on each other is presented in Figure 6 (a). It is also interesting to analyze the error E_{Cauchy} on the number of the elements in tetrahedral FEM mesh used in calculations. The latter dependence is shown in Figure 6 (b). Regarding Figure 6 (a) one can make a conclusion about stability of the algorithm (i.e., respective error of the solution depends regularly on the input data respective error). Figure 6 (b) is very common for inverse and ill-posed problems and shows the existence of the optimal number of elements (i.e., the mesh density).
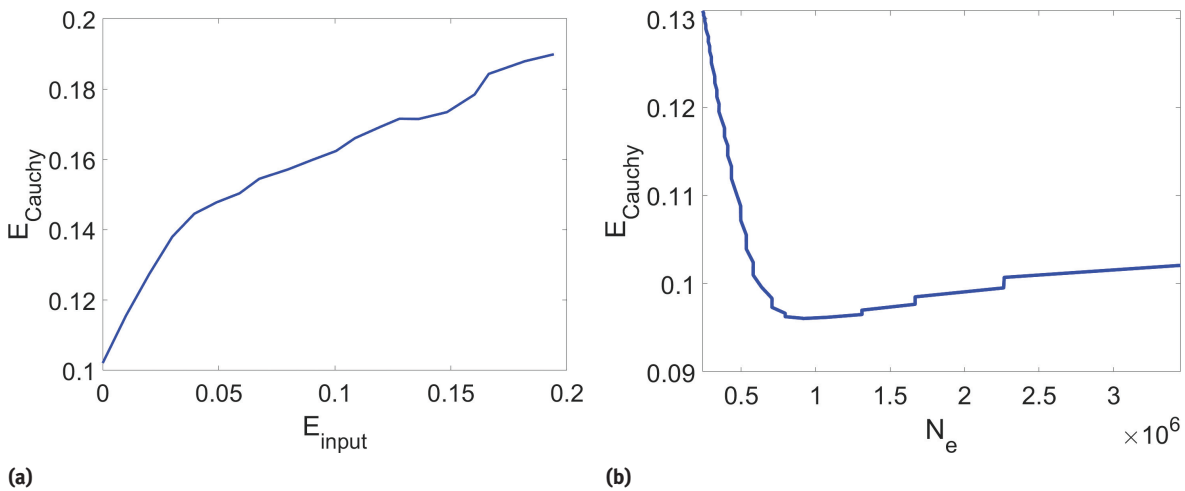

(a)   (b)

Figure 6: Error in the Cauchy solution in dependence of the error in input Cauchy data (a) and in dependence of the number of tetrahedra N_e in the FEM mesh (b).

Estimation of the depth of the source locations. The current paragraph aims to present the numerical results on Algorithm 1 together with other heuristic criteria (see Section 3.3). In order to do this, we constructed a simple model consisting of eight concentric spheres. Radii of the spheres and conductivities of the layers between them (chosen closed to real head conductivities) are presented in Table 1. The electric sources were

Radii, mm	100	97	94	91	88	85	70	68
σ_{het}, S/m	0.05	0.1	0.2	0.05	0.1	2.2	2.2	2.2
σ_{hom}, S/m	0.1	0.1	0.1	0.1	0.1	2.2	2.2	2.2

Table 1: Parameters of heterogeneous (σ_{het}) and homogeneous (σ_{hom}) models.
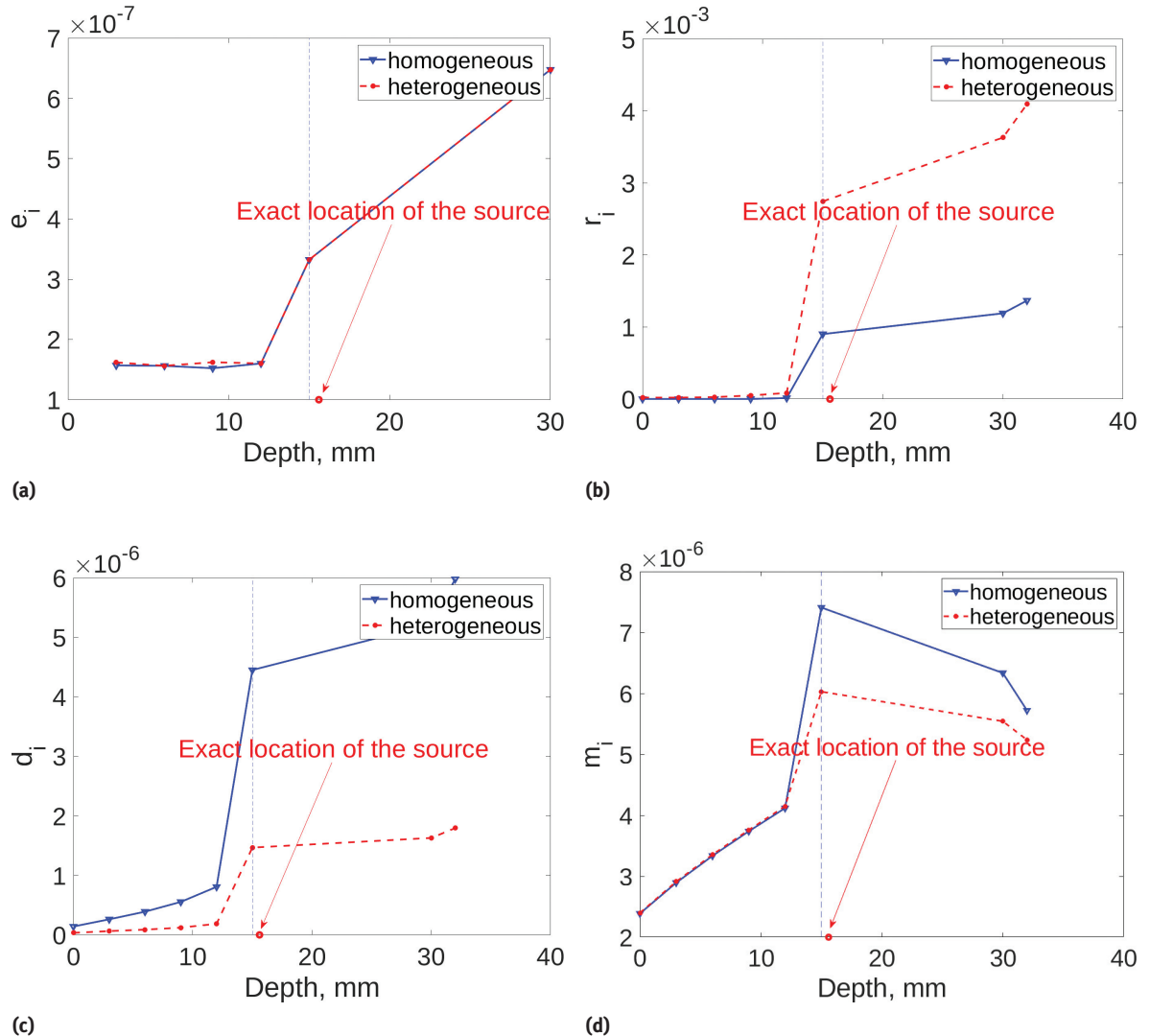

Figure 7: Dependencies on the depth of: (a) e_i, (b) relative residual r_i; (c) norm of Laplacian of the numerical solution d_i, and (d) maximum absolute values of the potential m_i.

located inside the layer between 6 and 7 sphere, on the depth 15.6 mm under the surface of the outer sphere. In order to make the experiment more vivid, we used two kinds of simulated data: the electric potential, simulated with the parameters listed above, and the electric potential simulated for the same geometry but with averaged conductivity of five outer (sourceless) layers equal to 0.1 S/m. All results, obtained with the first simulation (heterogeneous) are presented below, on Figure 7 with dashed red lines, while the numerical research for the second simulation (homogeneous) are presented with solid blue lines.

Figure 7 (a) depicts the usage of the main criterion described in Section 3.3. The exact depth of the electric source is equal to 15.6 mm and is presented with the red circle on the depth axis. Other heuristic criteria, based on generalized residual r_i, norms of ΔU_i, d_i, and the maximum of the absolute values of the potential m_i are shown in Figures 7 (b), (c), and (d), respectively. As one can see from the curves, although the values

for "homogeneous" and "heterogeneous" case differ, the behavior of all curves can be characterized by the jump of respective curves near the source.

5 Conclusion

In this paper, we presented an approach for scalp-to-cortex data mapping, based on the finite-element discretization. The method is based on solving the Cauchy problem for the Laplace's equation in homogeneous compartment and can be described as propagation of EEG from the scalp to the brain surface. Our numerical implementation employs the first-order finite-element approximation on tetrahedral grids, which can handle anatomical head models. The method can be considered as a pre-processing procedure, after which classical inverse source localization problem solvers can be applied. We believe the solution of the Cauchy problem described in this paper can be easily adapted to source localization in magnetoencephalography.

References

[1] F. Andersson, Evaluation of numerical techniques for solving the current injection problem in biological tissues, in: *IEEE International Symposium on Biomedical Imaging*, IEEE Press, Piscataway (2016), 876–880.

[2] S. Baillet, J. C. Mosher and R. M. Leahy, Electromagnetic brain mapping, *IEEE Trans. Signal Process. Mag.* **18** (2001), no. 6, 14–30.

[3] A. B. Bakushinskii, M. V. Klibanov and N. A. Koshev, Carleman weight functions for a globally convergent numerical method for ill-posed Cauchy problems for some quasilinear PDEs, *Nonlinear Anal. Real World Appl.* **34** (2017), 201–224.

[4] F. Berntsson and L. Eldén, Numerical solution of a Cauchy problem for the Laplace equation, *Inverse Problems* **17** (2001), no. 4, 839–853.

[5] L. Bourgeois, A mixed formulation of quasi-reversibility to solve the Cauchy problem for Laplace's equation, *Inverse Problems* **21** (2005), no. 3, 1087–1104.

[6] L. Bourgeois, Convergence rates for the quasi-reversibility method to solve the Cauchy problem for Laplace's equation, *Inverse Problems* **22** (2006), no. 2, 413–430.

[7] H. Cao, M. V. Klibanov and S. V. Pereverzev, A Carleman estimate and the balancing principle in the quasi-reversibility method for solving the Cauchy problem for the Laplace equation, *Inverse Problems* **25** (2009), no. 3, Article ID 035005.

[8] H. Cao and S. V. Pereverzev, The balancing principle for the regularization of elliptic Cauchy problems, *Inverse Problems* **23** (2007), no. 5, 1943–1961.

[9] M. Clerc and J. Kybic, Cortical mapping by Laplace–Cauchy transmission using a boundary element method, *Inverse Problems* **23** (2007), no. 6, 2589–2601.

[10] I. A. Corley and Y. Huang, Deep EEG super-resolution: Upsampling EEG spatial resolution with generative adversarial networks, in: *IEEE EMBS International Conference on Biomedical and Health Informatics* (BHI), IEEE Press, Piscataway (2018), 100–103.

[11] H. S. Courellis, J. R. Iversen, H. Poizner and G. Cauwenberghs, EEG channel interpolation using ellipsoid geodesic length, in: *IEEE Biomedical Circuits and Systems Conference*, IEEE Press, Piscataway (2016), 540–543.

[12] J. Dardé, A. Hannukainen and N. Hyvönen, An H_{div}-based mixed quasi-reversibility method for solving elliptic Cauchy problems, *SIAM J. Numer. Anal.* **51** (2013), no. 4, 2123–2148.

[13] J. C. De Munck, C. H. Wolters and M. Clerc, EEG and MEG: Forward modeling, in: *Handbook of Neural Activity Measurement*, Cambridge University, Cambridge (2012), 192–256.

[14] H. W. Engl and A. Leitão, A Mann iterative regularization method for elliptic Cauchy problems, *Numer. Funct. Anal. Optim.* **22** (2001), no. 7–8, 861–884.

[15] Q. Fang, Iso2mesh, 2018, http://iso2mesh.sourceforge.net/cgi-bin/index.cgi?Home.

[16] R. Grech, T. Cassar, J. Muscat, K. P. Camilleri, S. G. Fabri and M. Zervakis, Review on solving the inverse problem in EEG source analysis, *J. NeuroEng. Rehabilitation* **5** (2008), no. 25, 1–33.

[17] M. Hämäläinen, R. Hari, R. J. Ilmoniemi, J. Knuutila and O. V. Lounasmaa, Magnetoencephalography: Theory, instrumentation, and applications to noninvasive studies of the working human brain, *Rev. Modern Phys.* **65** (1993), no. 2, 413–497.

[18] M. Hämäläinen and R. J. Ilmoniemi, Interpreting magnetic fields of the brain: Minimum norm estimates, *Medical Biol. Eng. Comput.* **32** (1994), no. 1, 35–42.

[19] A. Hillebrand and G. R. Barnes, Beamformer analysis of MEG data, *Int. Rev. Neurobiology* **68** (2005), 149–171.

[20] M. V. Klibanov, N. A. Koshev, J. Li and A. G. Yagola, Numerical solution of an ill-posed Cauchy problem for a quasilinear parabolic equation using a Carleman weight function, *J. Inverse Ill-Posed Probl.* **24** (2016), no. 6, 761–776.

[21] M. V. Klibanov, N. A. Koshev, D.-L. Nguyen, L. H. Nguyen, A. Brettin and V. N. Astratov, A numerical method to solve a phaseless coefficient inverse problem from a single measurement of experimental data, *SIAM J. Imaging Sci.* **11** (2018), no. 4, 2339–2367.

[22] Y. A. Kuznetsov, O. V. Boiarkine, I. V. Kapyrin and N. B. Yavich, Numerical analysis of a two-level preconditioner for the diffusion equation with an anisotropic diffusion tensor, *Russian J. Numer. Anal. Math. Modelling* **22** (2007), no. 4, 377–391.

[23] J. Latikka, T. Kuurne and H. Eskola, Conductivity of living intracranial tissues, *Phys. Medicine Biol.* **46** (2001), 1611–1616.

[24] M. M. Lavrentyev, V. G. Romanov and S. P. Shishatsky, *Ill-posed Problems of Mathematical Physics and Analysis*, Nauka, Moscow, 1980.

[25] H. J. Li, X. S. Feng, J. Xiang and P. B. Zuo, New approach for solving the inverse boundary value problem of Laplace's equation on a circle: Technique renovation of the Grad-Shafranov (GS) reconstruction, *J. Geophys. Res. Space Phys.* **118** (2013), 1–7.

[26] F. H. Lin, T. Witzel, S. P. Ahlfors, S. M. Stufflebeam, J. W. Belliveau and M. S. Hämäläinen, Assessing and improving the spatial accuracy in MEG source localization by depth-weighted minimum-norm estimates, *NeuroImage* **31** (2006), no. 1, 160–171.

[27] H. McCann, G. Pisano and L. Beltrachini, Variation in reported human head tissue electrical conductivity values, *Brain Topography* **32** (2019), no. 5, 825–858.

[28] J. C. Mosher and R. M. Leahy, Recursive MUSIC: A framework for EEG and MEG source localization, *IEEE Trans. Biomedical Eng.* **45** (1998), no. 11, 1342–1354.

[29] I. Nouira, A. B. Abdallah and M. H. Bedoui, Potential mapping by 3D interpolation methods, in: *International Conference on Multimedia Computing and Systems* (ICMCS), IEEE Press, Piscataway (2014), 469–474.

[30] T. F. Oostendorp, The conductivity of the human skull: results of in vivo and in vitro measurements, *IEEE Trans. Biomedical Eng.* **47** (2000), 1487–1492.

[31] R. D. Pascual-Marqui, Standardized low-resolution brain electromagnetic tomography (sLORETA): Technical details, *Methods Find. Exp. Clinical Pharmacol. (Suppl. D)* **24** (2002), 5–12.

[32] R. D. Pascual-Marqui, C. M. Michel and D. Lehman, Low resolution electromagnetic tomography: A new method for localizing electrical activity in the brain, *Int. J. Psychophysiol.* **18** (1994), 49–65.

[33] R. Plonsey, *Biomagnetic Phenomena*, McGraw-Hill, New York, 1969.

[34] J. Sarvas, Basic mathematical and electromagnetic concepts of the biomagnetic inverse problem, *Phys. Medicine Biol.* **32** (1987), no. 1, 11–22.

[35] K. Sekihara and S. S. Nagarajan, *Adaptive Spatial Filters for Electromagnetic Brain Imaging*, Springer, Berlin, 2008.

[36] R. Srinivasan, P. L. Nunez, D. M. Tucker, R. B. Silberstein and P. J. Cadusch, Spatial sampling and filtering of EEG with spline laplacians to estimate cortical potentials, *Brain Topography* **8** (1996), no. 4, 355–366.

[37] B. D. V. Veen, W. van Drongelen, M. Yuchtman and A. Suzuki, Localization of brain electrical activity via linearity constrained minimum variance spatial filtering, *IEEE Trans. Biomedical Eng.* **44** (1977), no. 9, 867–880.

[38] T. V. Zakharova, P. I. Karpov and V. M. Bugaevskii, Localization of the activity source in the inverse problem of magnetoencephalography, *Comput. Math. Model.* **28** (2017), no. 2, 148–157.